JOURNAL OF AIRCRAFT
Vol. 46, No. 3, May–June 2009

Thermal Buckling and Flutter Behavior of Shape Memory Alloy Hybrid Composite Shells

Hesham Hamed Ibrahim,* Hong Hee Yoo,† and Kwan-Soo Lee‡
Hanyang University, Seoul 133-791, Republic of Korea

DOI: 10.2514/1.38787

A new nonlinear finite element formulation is presented to predict the thermal buckling and flutter boundaries of shape memory alloy hybrid composite cylindrical panels at elevated temperatures. The governing equations are obtained using Marguerre curved-plate theory and the principle of virtual work. The effect of large deflection is included in the formulation through the von Kármán nonlinear strain-displacement relations. To account for the temperature dependence of material properties, the thermal strain is stated as an integral quantity of the thermal expansion coefficient with respect to temperature. The aerodynamic pressure is modeled using the quasi-steady first-order piston theory. The Newton–Raphson iteration method is employed to obtain the nonlinear thermal postbuckling deflections, and a frequency-domain solution is presented to predict the critical dynamic pressure at elevated temperatures. Numerical results are presented to illustrate the effect of shape memory alloy fiber embeddings, temperature rise, height-to-thickness ratios, and boundary conditions on the panel response.

Nomenclature

$[A]$, $[B]$, $[D]$	=	in-plane, coupling, and bending matrices of a laminate
$[A_a]$	=	aerodynamic stiffness matrix
α	=	thermal expansion coefficient
$[G]$	=	aerodynamic damping matrix
H	=	maximum height rise
h	=	thickness
$[K]$, $[M]$	=	system linear stiffness and mass matrices
$[K_{\tan}]$	=	system tangent stiffness matrix
$\{N\}$, $\{M\}$	=	force and moment resultant vectors
$[N1]$, $[N2]$	=	system first- and second-order nonlinear stiffness matrices
$[\bar{Q}]$	=	transformed lamina reduced stiffness matrix
T_{ref}	=	reference temperature
V_s, V_m	=	volume fractions of the SMA fibers and the composite matrix
$\{W\}$	=	system nodal displacement vector
λ	=	nondimensional dynamic pressure
σ_r	=	Nitinol fiber recovery stress

Subscripts

b	=	bending
i	=	iteration number
m	=	membrane or composite matrix
r	=	due to recovery stress of Nitinol fibers
s	=	static or quantity related to SMA fibers
st	=	dependent on both static and dynamic displacements
t	=	dynamic or time-dependent
x, y, z	=	plate Cartesian coordinates

Received 28 May 2008; revision received 1 February 2009; accepted for publication 26 February 2009.

*Assistant Professor, Department of Mechanical Engineering; currently National Authority for Remote Sensing and Space Sciences, Cairo, 11769, Egypt; hhibrahim76@hotmail.com.

†Professor, Department of Mechanical Engineering, hhyoo@hanyang.ac.kr

‡Professor, Department of Mechanical Engineering, ksleehy@hanyang.ac.kr

I. Introduction

THE external skin of high-speed flight vehicles experiences high temperatures due to aerodynamic heating, which can induce thermal buckling and may result in a dynamic instability. In general, thermal buckling does not indicate structural failure. However, large thermal deflections of the skin panels can change the aerodynamic shape, affecting reduction in the flight performance. A comprehensive literature review on thermally induced flexure, buckling, and vibration of plates and shells was presented by Tauchart [1] and Thornton [2]. Gray and Mei [3] investigated the thermal postbuckling behavior and free vibration of thermally buckled composite plates using the finite element method. Shi et al. [4] presented a finite element solution for the thermal buckling behavior of laminated composite plates under combined mechanical and thermal loads. Eslami and Javaheri [5] investigated the buckling of composite cylindrical shells under mechanical and thermal loads. The governing equations were derived using Love–Kirchhoff hypothesis and Sander's nonlinear strain-displacement relations. Shen [6] presented a buckling analysis for functionally graded cylindrical thin shells subjected to external pressure and thermal environment. A singular perturbation technique was employed to determine the buckling loads and postbuckling equilibrium paths. Kadoli and Ganesan [7] investigated the linear thermal buckling and free vibration of functionally graded cylindrical shells. First-order shear deformation theories along with Fourier series expansion of the displacement variables were used to model the functionally graded material shell.

Panel flutter is a phenomenon that is usually accompanied by temperature elevation on the outer skin of high-speed air vehicles. Panel flutter is a self-excited oscillation of a plate or shell in supersonic flow. Because of aerodynamic pressure forces on the panel, two eigenmodes of the structure merge and lead to this dynamic instability. Panel flutter differs from wing flutter only in that the aerodynamic force resulting from the airflow acts only on one side of the panel. Thin plates are a commonly used form of structural components, especially in aerospace vehicles, such as high-speed aircraft, rockets, and spacecrafts, which are subjected to thermal loads due to aerodynamic and/or solar radiation heating. This results in a temperature distribution over the surface and thermal gradient through the thickness of the plate. The presence of these thermal fields results in a flutter motion at lower dynamic pressure or a larger limit-cycle amplitude at the same dynamic pressure. Accordingly, it is important to consider the interactive effect of both aforementioned failure characteristics (flutter and thermal buckling). A vast amount of literature exists on panel flutter using different structural and aerodynamic theories to model the structural response and the

aerodynamic pressure, respectively. Mei et al. [8] presented a review on the various analytical methods and experimental results of supersonic and hypersonic panel flutter. Ibrahim et al. [9] investigated the thermal buckling and flutter boundaries of thin functionally graded material plates at elevated temperature. They adopted an incremental finite element technique to capture the effect of the temperature dependence of material properties on the panel response. Ibrahim et al. [10] presented a finite element solution for the thermal buckling and nonlinear flutter performance of thin functionally graded material panels under combined aerodynamic and thermal loads. To account for the temperature dependence of material properties, the thermal strain was modeled as an integral quantity of thermal expansion coefficient with respect to temperature. Ibrahim et al. [11] extended the formulation presented in [10] by including the shear deformation effect to make it capable of handling thick functionally graded material plates. Singha and Mandal [12] investigated the supersonic flutter boundaries of composite cylindrical shell panels under combined aerodynamic and thermal environments. A 16-noded isoparametric degenerated shell element was employed along with the first-order high-Mach-number approximation to linear potential flow theory to evaluate the aerodynamic pressure. Haddadpour et al. [13] investigated the effect of temperature rise on the flutter boundaries of functionally graded cylindrical shells with simply supported edges. The aeroelastic equations of motion are constructed using Love's shell theory and von Kármán–Donnell type of kinematic nonlinearity coupled with linearized first-order potential (piston) theory.

Shape memory alloys (SMAs) have a unique ability to completely recover large prestrains (up to 10% elongation) when heated above a certain characteristic temperature. During the shape recovery process, a large tensile recovery stress occurs if the SMA is restrained. Both the recovery stresses and Young's modulus of SMA exhibit highly nonlinear temperature-dependent properties. Birman [14] presented a comprehensive review on the literature concerning SMA up to 1997. Lee et al. [15] investigated the thermal buckling behavior of laminated composite shells with embedded shape memory alloy wires. Modeling and buckling analysis were performed with the use of the ABAQUS code linked with a subroutine for the formulated SMA constitutive equations. Tawfik et al. [16] proposed a novel concept in enhancing the thermal buckling and aeroelastic behavior of plates through embedding SMA fibers in it. Park et al. [17] investigated the nonlinear vibration behavior of thermally buckled composite plates embedded with shape memory alloy fibers. An incremental method was adopted to account for the temperature-dependent material properties. Roh et al. [18] investigated the thermal postbuckling response of shape memory alloy hybrid composite shell panels. The layerwise displacement theory and the cylindrical arc length method were used in the formulation. Ibrahim et al. [19] investigated the thermal buckling and free-vibration behavior of thick, shape memory alloy hybrid composite plates. Moreover, a frequency-domain solution for predicting panel flutter boundaries at elevated temperatures was presented. Ibrahim et al. [20] investigated the nonlinear random response of moderately thick composite plates impregnated with prestrained shape memory alloy fibers under combined thermal and random acoustic loads. Ibrahim et al. [21] presented a new nonlinear finite element formulation to predict the aerothermal deflection and fundamental frequencies of SMA hybrid composite panels with initial sinusoidal geometric imperfection.

In the present paper, the nonlinear finite element formulation for the thermal buckling of shape memory alloy hybrid composite (SMAHC) plate panels employed earlier in [20] is extended to predict the thermal equilibrium paths of shape memory alloy hybrid composite shallow cylindrical shells. Moreover, for the first time in the literature, a frequency-domain solution along with Marguerre curved-plate theory is presented to predict the flutter boundaries of shape memory alloy hybrid composite cylindrical shells at elevated temperatures, taking into account the nonlinear stiffness added due to thermal deflection. The nonlinear governing equations for a thin, cylindrical rectangular panel are obtained using Marguerre curved-plate theory, von Kármán strain-displacement relations, and the principle of virtual work. To account for the temperature dependence of material properties, the thermal strain is modeled as an integral quantity of the thermal expansion coefficient with respect to temperature [9]. Numerical results are provided to show the effect of the temperature rise, prestrained SMA fiber embeddings, height-to-thickness ratios, and boundary conditions on the panel response.

II. Finite Element Formulation

A. Nonlinear Strain-Displacement Relations

The nodal degrees of freedom vector $\{\theta\}$ of a rectangular four-nodded Bogner–Fox–Schmidt (BFS) C^1 conforming plate element having 6 degrees of freedom at each node can be written as

$$\{\theta\} = \left\{\left\{w, \frac{\partial w}{\partial x}, \frac{\partial w}{\partial y}, \frac{\partial^2 w}{\partial x \partial y}\right\}, \{u, v\}\right\}^T = \begin{Bmatrix}\{w_b\}\\ \{w_m\}\end{Bmatrix} \tag{1}$$

where $\{w_b\}$ is the nodal transverse displacement and rotations vector and $\{w_m\}$ is the nodal membrane displacements vector. Consider the cylindrical panel surface w_o and the lateral deflection w shown in Fig. 1; the Marguerre curved-plate strain-displacement relation along with von Kármán large deflection can be written as [22]

$$\begin{Bmatrix}\varepsilon_x\\ \varepsilon_y\\ \gamma_{xy}\end{Bmatrix} = \begin{Bmatrix}\frac{\partial u}{\partial x}\\ \frac{\partial v}{\partial y}\\ \frac{\partial u}{\partial y}+\frac{\partial v}{\partial x}\end{Bmatrix} + \begin{Bmatrix}\frac{1}{2}\left(\frac{\partial w}{\partial x}\right)^2\\ \frac{1}{2}\left(\frac{\partial w}{\partial y}\right)^2\\ \frac{\partial w}{\partial x}\frac{\partial w}{\partial y}\end{Bmatrix} + \begin{Bmatrix}\frac{\partial w}{\partial x}\frac{\partial w_o}{\partial x}\\ \frac{\partial w}{\partial y}\frac{\partial w_o}{\partial y}\\ \frac{\partial w}{\partial x}\frac{\partial w_o}{\partial y}+\frac{\partial w_o}{\partial x}\frac{\partial w}{\partial y}\end{Bmatrix} + \bar{z}\begin{Bmatrix}-\frac{\partial^2 w}{\partial x^2}\\ -\frac{\partial^2 w}{\partial y^2}\\ -2\frac{\partial^2 w}{\partial x \partial y}\end{Bmatrix} \tag{2}$$

or in a compact form as

$$\{\varepsilon\} = \{\varepsilon_m^o\} + \{\varepsilon_b^o\} + \{\varepsilon_{wo}^o\} + \bar{z}\{\kappa\} \tag{3}$$

where $\{\varepsilon_m^o\}$, $\{\varepsilon_b^o\}$, $\{\varepsilon_{wo}^o\}$, and $\bar{z}\{\kappa\}$ are the membrane linear strain vector, the membrane nonlinear strain vector, the in-plane strain vector due to panel curvature, and the bending strain vector, respectively. The local coordinate $\bar{z}$ is defined as $\bar{z} = z - w_o$. In addition, the cylindrical panel adopted in this study is assumed to have a constant radius in the x direction and an infinite radius in the y direction, and the cylindrical curved surface $w_o(x)$ may be approximated by the following form [22]:

$$w_o(x) = H\left(1 - \frac{(x-(a/2))^2}{(a/2)^2}\right) \tag{4}$$

where H is the maximum height rise and a are the plate dimension along the x direction.

B. Constitutive Equations

For the kth composite lamina impregnated with SMA fibers, the stress–strain relations can be expressed as [20]

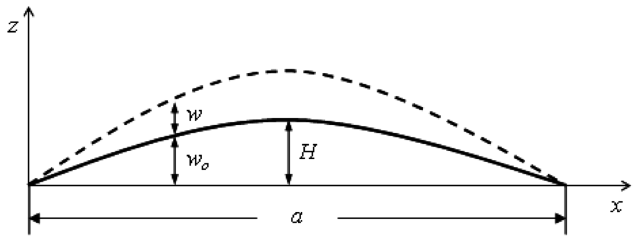

Fig. 1 Schematic for the initial cylindrical surface w_o and the transverse deflection w.

$$\{\sigma^k\} = \begin{Bmatrix} \sigma_x^k \\ \sigma_y^k \\ \tau_{xy}^k \end{Bmatrix} = [\bar{Q}^k(T)]\{\varepsilon\} - \int_{T_{\text{ref}}}^{T} [\bar{Q}^k(\tau)]\{\alpha^k(\tau)\}\mathrm{d}\tau, \qquad T < A_s$$

$$\{\sigma^k\} = \begin{Bmatrix} \sigma_x^k \\ \sigma_y^k \\ \tau_{xy}^k \end{Bmatrix} = [\bar{Q}^k(T)]\{\varepsilon\} + V_s^k\{\sigma_r^k(T)\} - V_m^k \int_{T_{\text{ref}}}^{T} [\bar{Q}_m^k(\tau)]\{\alpha_m^k(\tau)\}\mathrm{d}\tau, \qquad T \geq A_s \tag{5}$$

where $\{\sigma\}$ and $\{\sigma_r\}$ are the in-plane and the SMA recovery-stress vectors at a given temperature T; V_m and V_s are the volume fractions of the composite matrix and SMA fibers, respectively; A_s is the austenite start temperature; and $\{\alpha_m\}$, $[\bar{Q}]$, and $[\bar{Q}_m]$ are the thermal expansion coefficient vector of the composite matrix, the transformed reduced stiffness matrix of the SMAHC lamina, and the transformed reduced stiffness matrix of the composite matrix, respectively. Note that the SMA fibers are embedded in the same direction as the composite matrix fibers and assumed to be uniformly distributed within each layer. Integrating Eq. (5) over the panel thickness h, the constitutive equation is obtained as

$$\begin{Bmatrix} \{N\} \\ \{M\} \end{Bmatrix} = \begin{bmatrix} [A] & [B] \\ [B] & [D] \end{bmatrix} \begin{Bmatrix} \{\varepsilon_m^o\} + \{\varepsilon_b^o\} + \{\varepsilon_{wo}^o\} \\ \{\kappa\} \end{Bmatrix} - \begin{Bmatrix} \{N_T\} \\ \{M_T\} \end{Bmatrix} + \begin{Bmatrix} \{N_r\} \\ \{M_r\} \end{Bmatrix} \tag{6}$$

where

$$\begin{Bmatrix} N_T \\ M_T \end{Bmatrix} = \int_{-h/2}^{h/2} \left[\left(\int_{T_{\text{ref}}}^{T} [Q(\tau)]\{\alpha(\tau)\}\mathrm{d}\tau \right) \right] \begin{Bmatrix} 1 \\ z \end{Bmatrix} \mathrm{d}z, \qquad T < A_s$$

$$\begin{Bmatrix} N_T \\ M_T \end{Bmatrix} = V_m \int_{-h/2}^{h/2} \left[\left(\int_{T_{\text{ref}}}^{T} [Q_m(\tau)]\{\alpha_m(\tau)\}\mathrm{d}\tau \right) \right] \begin{Bmatrix} 1 \\ z \end{Bmatrix} \mathrm{d}z, \qquad T \geq A_s$$

$$\begin{Bmatrix} N_r \\ M_r \end{Bmatrix} = 0, \quad T < A_s \qquad \begin{Bmatrix} N_r \\ M_r \end{Bmatrix} = V_s \int_{-h/2}^{h/2} \{\sigma_r\} \begin{Bmatrix} 1 \\ z \end{Bmatrix} \mathrm{d}z, \quad T \geq A_s$$

C. Aerodynamic Pressure Loading

The first-order quasi-steady piston theory for supersonic flow states that [16]

$$P_a = -\left(\frac{g_a}{\omega_o} \frac{D_{110}}{a^4} \frac{\partial(w + w_o)}{\partial t} + \lambda \frac{D_{110}}{a^3} \frac{\partial(w + w_o)}{\partial x} \right) \tag{7}$$

with

$$g_a = \frac{\rho_a \nu (M_\infty^2 - 2)}{\rho h \omega_o \beta^3} = \sqrt{\lambda C_a}, \qquad C_a = \frac{(M_\infty^2 - 2)^2}{(M_\infty^2 - 1)^2} \frac{\rho_a a}{\rho h \beta}$$

$$\lambda = \frac{2qa^3}{\beta D_{110}}, \qquad q = \frac{\rho_a \nu^2}{2}, \qquad \beta = \sqrt{M_\infty^2 - 1}, \quad \text{and} \quad \omega_o = \left(\frac{D_{110}}{\rho h a^4} \right)^{\frac{1}{2}}$$

where P_a is the aerodynamic pressure loading, ν is the airflow velocity on one side of the panel, M_∞ is the Mach number, q is the dynamic pressure, ρ_a is the air mass density, g_a is the nondimensional aerodynamic damping, C_a is the aerodynamic damping coefficient, λ is the nondimensional dynamic pressure, D_{110} is the first entry in the flexural stiffness matrix D (1, 1) when all the fibers of the composite layers are aligned in the airflow x direction, and a is the streamwise panel length.

D. Governing Equations

The principle of virtual work states that

$$\delta\text{work} = \delta\text{work}_{\text{int}} - \delta\text{work}_{\text{ext}} = 0 \tag{8}$$

where the virtual work done by internal stresses can be written as

$$\begin{aligned} \delta\text{work}_{\text{int}} &= \int_A (\{\delta(\{\varepsilon_m^o\} + \{\varepsilon_b^o\} + \{\varepsilon_{wo}^o\})\}^T\{N\} + \{\delta\kappa\}^T\{M\})\mathrm{d}A \\ &= \{\delta\theta\}^T \left([k] + [k_{wo}] - [k_T] + [k_r] + \frac{1}{2}([n1] + [n1_{wo}]) + \frac{1}{3}[n2] \right) \{\theta\} - \{\delta\theta\}^T(\{p_T\} + \{p_{Two}\} - \{p_r\} - \{p_{rwo}\}) \end{aligned} \tag{9}$$

where $[k]$, $[k_T]$, and $[k_r]$ are the linear, thermal, and recovery-stress stiffness matrices; $[k_{wo}]$ is a linear stiffness matrix due to initial cylindrical panel geometry w_o; $[n1]$ and $[n2]$ are the first- and second-order nonlinear stiffness matrices, respectively; $[n1_{wo}]$ is a first-order stiffness matrix due to cylindrical panel geometry; $\{p_T\}$ and $\{p_r\}$ are thermal and recovery-stress load vectors; and $\{p_{Two}\}$ and $\{p_{rwo}\}$ are thermal and recovery load vectors due to cylindrical panel geometry. On the other hand, the external virtual work $\delta\text{work}_{\text{ext}}$ can be stated as follows [9]:

$$\begin{aligned} \delta\text{work}_{\text{ext}} &= \int_A \left(\delta w \left(-\rho h \frac{\partial^2 w}{\partial t^2} + P_a \right) + \delta u \left(-\rho h \frac{\partial^2 u}{\partial t^2} \right) + \delta v \left(-\rho h \frac{\partial^2 v}{\partial t^2} \right) \right) \mathrm{d}A \\ &= -\{\delta\theta\}^T \begin{bmatrix} m_b & 0 \\ 0 & m_m \end{bmatrix} \{\ddot{\theta}\} - \{\delta\theta\}^T \begin{bmatrix} g_b & 0 \\ 0 & 0 \end{bmatrix} \{\dot{\theta}\} - \{\delta\theta\}^T \lambda \begin{bmatrix} a_{ab} & 0 \\ 0 & 0 \end{bmatrix} \{\theta\} - \{\delta\theta\}^T \lambda \begin{Bmatrix} p_b^{\text{sal}} \\ 0 \end{Bmatrix} \\ &= -\{\delta\theta\}^T[m]\{\ddot{\theta}\} - \{\delta\theta\}^T[g]\{\dot{\theta}\} - \{\delta\theta\}^T\lambda[a_a]\{\theta\} - \{\delta\theta\}^T\lambda\{p^{\text{sal}}\} \end{aligned} \tag{10}$$

where

$$\lambda[a_{ab}] = \lambda \frac{D_{110}}{a^3} \int_A \left(\delta w \left(\frac{\partial w}{\partial x} \right) \right) \mathrm{d}A$$

$$[g_b] = \frac{g_a}{\omega_o} \frac{D_{110}}{a^4} \int_A \left(\delta w \left(\frac{\partial w}{\partial t} \right) \right) \mathrm{d}A$$

$$\lambda\{p_b^{\text{sal}}\} = \lambda \frac{D_{110}}{a^3} \int_A \left(\delta w \left(\frac{\partial w_o}{\partial x} \right) \right) \mathrm{d}A$$

where $[m]$, $[g]$, and $[a_a]$ are mass, aerodynamic damping, and aerodynamic stiffness matrices, respectively; $\{p^{\text{sal}}\}$ is a static aerodynamic load vector, which is function of the initial cylindrical panel geometry w_o. By substituting Eqs. (9) and (10) into Eq. (8), the governing equations for a shape memory alloy hybrid composite cylindrical panel under the combined action of thermal and aerodynamic loads can be written as

$$\begin{aligned} &[M]\{\ddot{W}\} + [G]\{\dot{W}\} + (\lambda[A_a] + [K] + [K_{wo}] - [K_T] + [K_r] \\ &\quad + \tfrac{1}{2}([N1] + [N1_{wo}]) + \tfrac{1}{3}[N2])\{W\} \\ &\quad = \{P_T\} + \{P_{Two}\} - \{P_r\} - \{P_{rwo}\} - \lambda\{P^{\text{sal}}\} \end{aligned} \tag{11}$$

III. Solution Procedures

The solution of the system of ordinary differential equations presented in Eq. (11) can be separated as the sum of a time-independent particular solution and a time-dependent homogenous solution. The total deflection can be written as

$$\{W\} = \{W\}_s + \{W\}_t \tag{12}$$

The particular solution characterizes a static thermal postbuckling deflection $\{W\}_s$, and the homogenous solution characterizes a self-exited dynamic flutter oscillation $\{W\}_t$ about the static equilibrium position $\{W\}_s$. Substituting Eq. (12) into Eq. (11) results in the following:

$$[M]\{\ddot{W}\}_t + [G]\{\dot{W}\}_t + (\lambda[A_a] + [K] + [K_{wo}] - [K_T] + [K_r] + \tfrac{1}{2}([N1]_{s+t}) + \tfrac{1}{2}[N1_{wo}]_{s+t} + \tfrac{1}{3}[N2]_{s+t})(\{W\}_s + \{W\}_t) = \{P_T\} + \{P_{Two}\} - \{P_r\} - \{P_{rwo}\} - \lambda\{P^{\text{sal}}\} \quad (13)$$

where the subscript $(s + t)$ denotes that the corresponding nonlinear stiffness matrix is evaluated using the total deflection. Equation (13) can be separated into static and dynamic equations as follows [11]:

$$(\lambda[A_a] + [K] + [K_{wo}] - [K_T] + [K_r] + \tfrac{1}{2}([N1]_s + [N1_{wo}]_s) + \tfrac{1}{3}[N2]_s)\{W\}_s = \{P_T\} + \{P_{Two}\} - \{P_r\} - \{P_{rwo}\} - \lambda\{P^{\text{sal}}\} \quad (14)$$

$$[M]\{\ddot{W}\}_t + [G]\{\dot{W}\}_t + (\lambda[A_a] + [K] + [K_{wo}] - [K_T] + [K_r] + \tfrac{1}{2}([N1]_t) + \tfrac{1}{2}[N1_{wo}]_t + \tfrac{1}{3}[N2]_t)\{W\}_t + ([N1]_s + [N1_{wo}]_s + [N2]_s + [N2]_{st})\{W\}_t = \{0\} \quad (15)$$

A. Aerothermal Deflection

For the thermal postbuckling problem, the solution procedure using the Newton–Raphson iteration method is presented in the following. Introducing the function $\{\Psi(W)\}$ to Eq. (14) to be

$$\{\Psi(W_s)\} = (\lambda[A_a] + [K] + [K_{wo}] - [K_T] + [K_r] + \tfrac{1}{2}([N1]_s + [N1_{wo}]_s) + \tfrac{1}{3}[N2]_s)\{W\}_s - \{P_T\} - \{P_{Two}\} + \{P_r\} + \{P_{rwo}\} + \lambda\{P^{\text{sal}}\} = 0 \quad (16)$$

Equation (16) can be written in the form of a truncated Taylor series as

$$\{\Psi(W_s + \delta W)\} = \{\Psi(W_s)\} + \frac{d\{\Psi(W_s)\}}{d(W_s)}\{\delta W\} \cong 0 \quad (17)$$

where [11]

$$\frac{d\{\Psi(W_s)\}}{d(W_s)} = (\lambda[A_a] + [K] + [K_{wo}] - [K_T] + [K_r] + [N1]_s + [N1_{wo}]_s + [N2]_s) = [K_{\tan}] \quad (18)$$

Thus, the Newton–Raphson iteration procedure for the determination of the thermal postbuckling deflection can be expressed as follows:

$$\{\Psi(W_s)\}_i = (\lambda[A_a] + [K] + [K_{wo}] - [K_T] + [K_r] + \tfrac{1}{2}([N1]_s + [N1_{wo}]_s)_i + \tfrac{1}{3}([N2]_s)_i)(\{W\}_s)_i - \{P_T\} - \{P_{Two}\} + \{P_r\} + \{P_{rwo}\} + \lambda\{P^{\text{sal}}\}$$

$$[K_{\tan}]_i\{\delta W\}_{i+1} = -\{\Psi(W_s)\}_i$$

$$\{\delta W\}_{i+1} = -[K_{\tan}]^{-1}\{\Psi(W_s)\}_i$$

$$\{W_s\}_{i+1} = \{W_s\}_i + \{\delta W\}_{i+1}$$

Convergence occurs in the preceding procedure when the maximum value of $\{\delta W\}_{i+1}$ becomes less than a given tolerance ε_{tol} (i.e., $\max|\{\delta W\}_{i+1}| \le \varepsilon_{\text{tol}}$).

B. Flutter Boundaries at Elevated Temperatures

In this section, the procedure of determining the critical nondimensional dynamic pressure at elevated temperatures is presented. By assuming $\{W\}_t \ll 1$, all the dynamic nonlinear terms will be dropped from Eq. (15) and the linearized dynamic equation of motion that represents the flutter boundary at elevated temperatures can be stated as follows:

$$[M]\{\ddot{W}\}_t + [G]\{\dot{W}\}_t + (\lambda[A_a] + [K] + [K_{wo}] - [K_T] + [K_r] + [N1]_s + [N1_{wo}]_s + [N2]_s)\{W\}_t = \{0\} \quad (19)$$

Or

$$\begin{bmatrix} M_b & 0 \\ 0 & M_m \end{bmatrix}\begin{Bmatrix} \ddot{W}_b \\ \ddot{W}_m \end{Bmatrix}_t + \begin{bmatrix} G_b & 0 \\ 0 & 0 \end{bmatrix}\begin{Bmatrix} \dot{W}_b \\ \dot{W}_m \end{Bmatrix}_t + \left(\lambda\begin{bmatrix} A_{ab} & 0 \\ 0 & 0 \end{bmatrix} + \begin{bmatrix} K_b & K_{bm} \\ K_{mb} & K_m \end{bmatrix} + \begin{bmatrix} K_{wob} & K_{wobm} \\ K_{womb} & 0 \end{bmatrix} - \begin{bmatrix} K_{Tb} & 0 \\ 0 & 0 \end{bmatrix} + \begin{bmatrix} K_{rb} & 0 \\ 0 & 0 \end{bmatrix} + \begin{bmatrix} N1_b + N1_{wob} & N1_{bm} \\ N1_{mb} & 0 \end{bmatrix}_s + \begin{bmatrix} N2_b & 0 \\ 0 & 0 \end{bmatrix}_s\right)\begin{Bmatrix} W_b \\ W_m \end{Bmatrix}_t = \begin{Bmatrix} 0 \\ 0 \end{Bmatrix} \quad (20)$$

Neglecting the in-plane inertia term will not bring significant error, because their natural frequencies are usually 2 to 3 orders of magnitude higher than the bending ones [20]. Separating Eq. (20) in the membrane and transverse directions results in the following:

$$[M_b]\{\ddot{W}_b\}_t + [G_b]\{\dot{W}_b\}_t + (\lambda[A_{ab}] + [K_b] + [K_{wo_b}] - [K_{Tb}] + [K_{rb}] + [N1_b + N1_{wob}]_s + [N2_b]_s)\{W_b\}_t + ([K_{bm}] + [K_{wobm}] + [N1_{bm}]_s)\{W_m\}_t = \{0\} \quad (21)$$

$$([K_{mb}] + [K_{womb}] + [N1_{mb}]_s)\{W_b\}_t + [K_m]\{W_m\}_t = \{0\} \quad (22)$$

Substituting Eq. (22) into Eq. (21) results in the following linearized transverse dynamic equation:

$$[M_b]\{\ddot{W}_b\}_t + [G_b]\{\dot{W}_b\}_t + (\lambda[A_{ab}] + [K_b] + [K_{wo_b}] - [K_{Tb}] + [K_{rb}] + [N1_b + N1_{wob}]_s + [N2_b]_s)\{W_b\}_t - ([K_{bm}] + [K_{wobm}] + [N1_{bm}]_s)([K_m]^{-1}[K_{mb}] + [K_m]^{-1}[K_{womb}] + [K_m]^{-1}[N1_{mb}]_s)\{W_b\}_t = \{0\} \quad (23)$$

Now, assuming the deflection function of the transverse displacement $\{W_b\}_t$ to be in the form

$$\{W_b\}_t = \bar{c}\{\Phi_b\}e^{\Omega t} \quad (24)$$

where $\Omega = \alpha + i\omega$ is the complex panel motion parameter (α is the damping ratio and ω is the frequency), $\bar{c}$ is the amplitude of vibration, and $\{\Phi_b\}$ is the mode shape. Substituting Eq. (24) into Eq. (23), the generalized eigenvalue problem can be stated as

$$\bar{c}[\kappa[M] + [\bar{K}]]\{\Phi_b\}e^{\Omega t} = \{0\} \quad (25)$$

where

$$\kappa = \Omega^2 + \omega_o g_a \Omega$$

$$[\bar{K}] = (\lambda[A_{ab}] + [K_b] + [K_{wo_b}] - [K_{Tb}] + [K_{rb}] + [N2_b]_s + [N1_b + N1_{wob}]_s) - ([K_{bm}][K_m]^{-1}[K_{mb}] + [K_{wobm}][K_m]^{-1}[K_{mb}] + [N1_{bm}]_s[K_m]^{-1}[K_{mb}] + [K_{bm}][K_m]^{-1}[K_{womb}] + [K_{wobm}][K_m]^{-1}[K_{womb}] + [N1_{bm}]_s[K_m]^{-1}[K_{womb}] + [K_{bm}][K_m]^{-1}[N1_{mb}]_s + [K_{wobm}][K_m]^{-1}[N1_{mb}]_s + [N1_{bm}]_s[K_m]^{-1}[N1_{mb}]_s)$$

From Eq. (25), we can write the generalized eigenvalue problem as

$$[-\kappa[M_b] + [\bar{K}]]\{\Phi_b\} = \{0\} \quad (26)$$

where κ is the eigenvalue and Φ_b is the mode shape vector of the following characteristic equation:

$$|-\kappa[M_b] + [\bar{K}]| = \{0\} \quad (27)$$

Table 1 Material properties for both the composite matrix and the Nitinol fibers

Nitinol		Graphite-epoxy	
Properties	Values	Properties	Values
See Fig. 2 for Young's modulus.		$E1$	$155\,(1-6.35\times10^{-4}\Delta T)$ GPa
See Fig. 3 for recovery stresses.		$E2$	$8.07\,(1-7.69\times10^{-4}\Delta T)$ GPa
G	25.6 GPa	$G12$	$4.55\,(1-1.09\times10^{-3}\Delta T)$ GPa
ρ	6450 kg/m^3	ρ	1550 kg/m^3
ν	0.3	ν	0.22
α	10.26×10^{-6}/°C	$\alpha1$	$-0.07\times10^{-6}(1-0.69\times10^{-3}\Delta T)$/°C
		$\alpha2$	$30.6\times10^{-6}(1+0.28\times10^{-4}\Delta T)$/°C

Given that the values of κ are real for all values of λ below the critical value, an iterative solution can be used to determine the value of the critical nondimensional dynamic pressure λ_{cr}.

IV. Numerical Results and Discussions

This section presents numerical results for the thermal postbuckling deflections and the flutter boundaries at elevated temperatures of a laminated composite cylindrical panel with and without SMA fibers. Convergence was found to occur at a uniform 8×8 finite element mesh of a rectangular four-noded BFS C^1 conforming plate element and thus used. The dimensions of the composite cylindrical panel adopted throughout this study, unless specified otherwise, are $0.381\times0.305\times0.0013$ (m) and the stacking sequence is $[0/-45/45/90]_s$. The four edges of the panel will be all simply supported or all clamped. Table 1 presents the material properties of both composite matrix and SMA fibers [20], and the variation of the modulus of elasticity and recovery stress of a trained SMA fibers, made from Nitinol, are presented in Figs. 2 and 3 [23]. SMA fibers are evenly distributed in each lamina and aligned in the same direction as the graphite fibers of the graphite-epoxy composite matrix. Uniform temperature change was applied to the plate, and the reference temperature was assumed to be 21°C.

The thermal postbuckling deflection of a simply supported, eight-layered $[0/-45/45/90]_s$, graphite-epoxy cylindrical shallow shell of rectangular plan form is presented in Fig. 4. The in-plane conditions are immovable at all four edges. The shell is of $0.356\times0.254\times0.001$ m, it has a constant radius in the x direction $R_x/a=40$, and R_y is infinity. To verify the present formulation, the results presented in Fig. 4 were compared with those of Fig. 2 in [24] and were found to be in a good agreement.

Figures 5 and 6 present the thermal postbuckling equilibrium paths for a clamped cylindrical panel, illustrating the effect of both SMA fiber embeddings and height-to-thickness ratio H/h on the panel response. Figure 5 presents the thermal buckling of a clamped composite cylindrical panel with different height-to-thickness ratios. It is seen that there is no sudden out-of-plane deflection (i.e., buckling phenomenon), because any small temperature rise results in a prompt transverse deflection of the panel due to the initial curvature of the panel, which makes all curved panels lose their distinct critical buckling temperature. Therefore, the cylindrical panels have superior performance at elevated temperatures, except at the temperature rises less than 22.5°C (i.e., before the buckling point of the clamped composite-plate panel). It is also seen that increasing H/h value has a favorable effect on the panel response through decreasing the postbuckling deflection, especially at high temperatures, as a result of the stiffness added due to panel curvature. Figure 6 presents the thermal buckling of a clamped SMAHC cylindrical panel with 10% SMA volume fraction and a prestrain of 3%. For the panels having $H/h=0$, it is seen that SMA fiber embeddings result in highly increasing the buckling temperature and decreasing or suppressing the postbuckling deflection, compared with the composite-plate panel response. At temperature rises ΔT lower than 103°C, the tension field generated by the shape-constrained shape recovery process of the SMA fibers is found to totally dominate the thermal stresses, resulting in decreasing the panel height. This decrease in panel height may adversely affect the aerodynamic performance, but the SMAHC cylindrical panels deflections are still lower than those of the composite cylindrical panels shown in Fig. 5. Because the constrained shape recovery load vector due to cylindrical panel geometry $\{P_{rwo}\}$ increases with increasing H/h, the SMAHC panel with $H/h=3$ is found to have higher deflections than those of the $H/h=1$ panel at ΔT lower than 103°C. At ΔT higher than 103°C, the thermal stresses is found to dominate the SMA recovery stresses, resulting in an outward deflection that is decreasing with increasing the panel height. At ΔT lower than 137°C (i.e., less than the critical buckling temperature of the SMAHC plate panel), The SHAHC plate panel response is found to be better than the SMAHC cylindrical panels regarding shape stability.

Figures 7 and 8 depict the aerothermal centerline deflections in the x direction for a clamped composite cylindrical panel with $H/h=1$, $\Delta T=20$°C, and at various dynamic pressures λ. Figure 7 shows a gradual evolution of the aerothermal deflection as the dynamic pressure λ is increasing. As the value of λ is progressively raised, a portion of the aerothermal deflection is found to move toward the

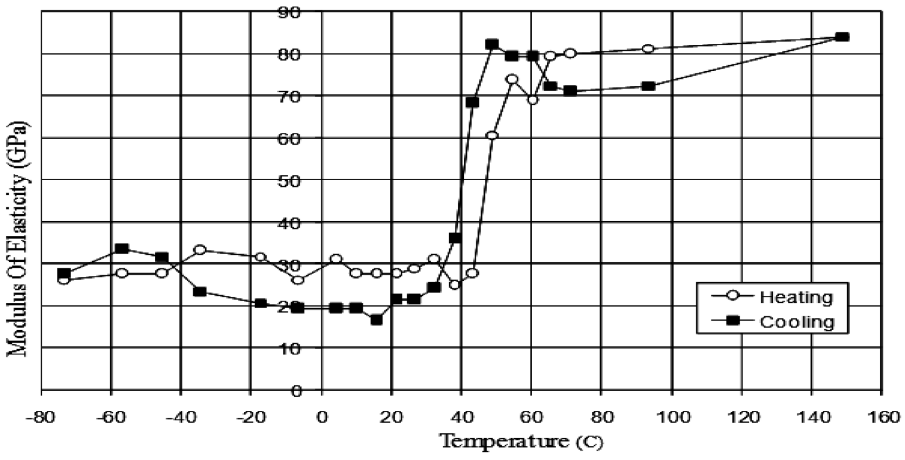

Fig. 2 Modulus of elasticity variation with temperature for a trained Nitinol fiber.

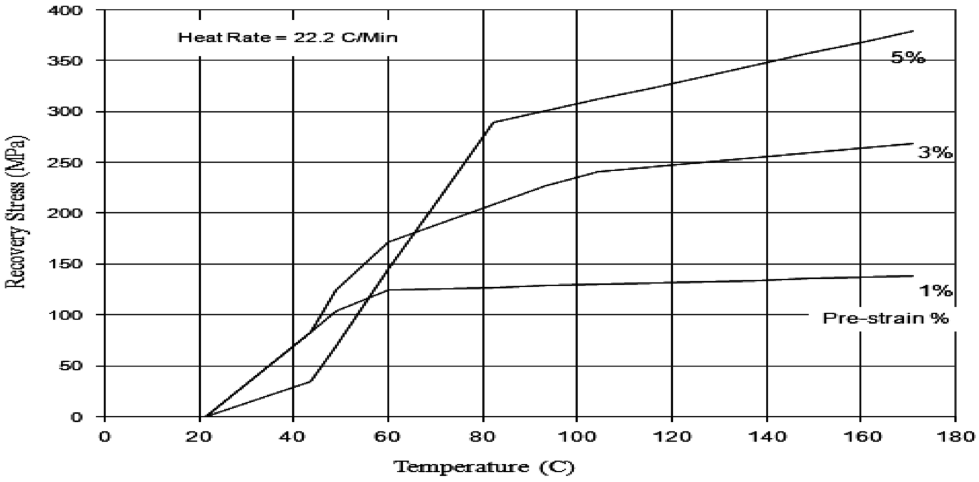

Fig. 3 Nitinol recovery stress as a function of both temperature and prestrain percentage.

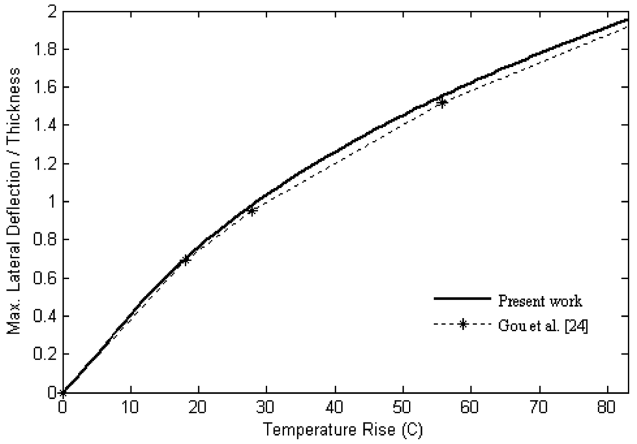

Fig. 4 Maximum nondimensional thermal deflection of a simply supported composite cylindrical shallow shell.

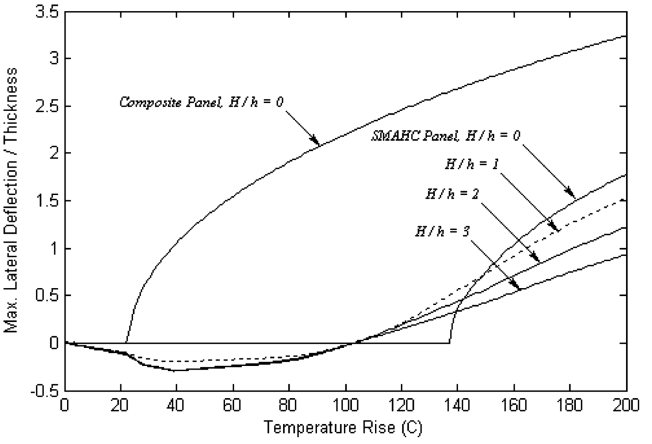

Fig. 6 Maximum nondimensional thermal deflection of a clamped SMAHC cylindrical panel with SMA volume fraction 10% and prestrain 3%.

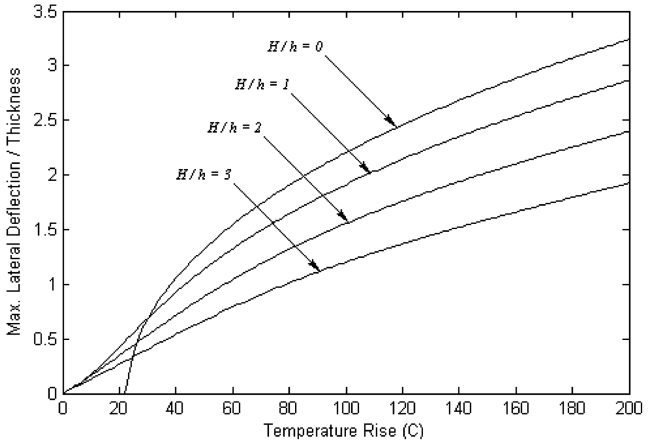

Fig. 5 Maximum nondimensional thermal deflection of a clamped composite cylindrical panel with different height-to-thickness ratios H/h.

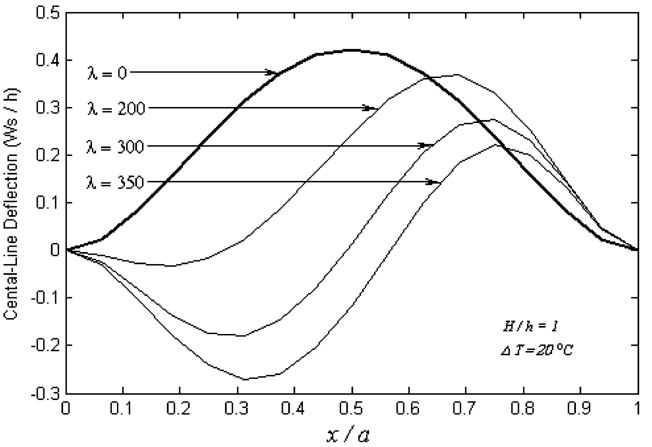

Fig. 7 Aerothermal deflection of a clamped composite cylindrical panel with $H/h = 1$, $\Delta T = 20°\mathrm{C}$ and different λ.

negative side, and the maximum panel's peak is gradually shifting toward the trailing edge with lower height, as shown in Fig. 8.

It is obvious that the flutter behavior of the curved panels would behave differently from the flat panels' behavior. Whereas there is no perceptible aerostatic deflection for flat panels in the preflutter region, the curved panel exhibits a clear aerostatic deflection, depending on the dynamic pressure λ and the height rise H/h. An important step toward the computation of the cylindrical panels' stability boundaries is the determination of the preflutter aerothermal deflection $\{W\}_s$. The investigation of the natural frequencies of the deflected curved panel under the influence of the static aerodynamic load as a function of the dynamic pressure λ and panel curvature could lead to the coalescence of two aerostatic eigenmodes subsequently allowing the determination of the flutter onset [22].

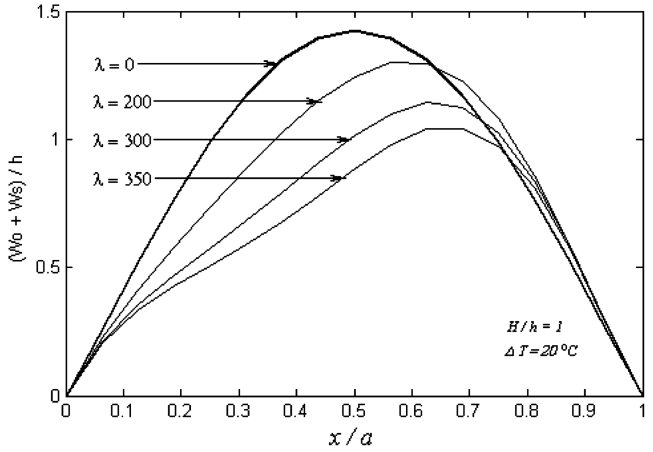

Fig. 8 Cylindrical panel geometries with $H/h = 1$, $\Delta T = 20°\text{C}$ and different λ.

Figure 9 illustrates the flutter coalescence curve for a composite cylindrical panel with $H/h = 1$ and $\Delta T = 0°\text{C}$. The figure shows a gradual hardening of the aerostatic mode 1, whereas the aerostatic mode 2 experiences a light hardening then a steep softening toward the softening region until the coalescence with mode 1 in the hardening region at $\lambda_{cr} = 563$. Figure 10 presents a comparison between the flutter boundaries of clamped composite and SMAHC flat panels. The critical flutter dynamic pressure λ_{cr} of the composite panel is seen to decrease with temperature rise until reaching $\Delta T = 45°\text{C}$, whereas no convergence is attained for $\{W\}_s$ in the Newton–Raphson iterative process, as the panel might be experiencing snap-through motion or chaotic limit-cycle oscillation [22]. Figure 3 shows that in the temperature rise range of 21–43°C, the 5% prestrain curve has a slower rate of recovery-stress rise with temperature than that of the 3% prestrain. This makes the thermal stress dominates the SMA recovery stress during this temperature range, and hence, the critical dynamic pressure decreases steeply with temperature rise, until the occurrence of buckling, compared with the 3% prestrain curve shown in Fig 10. It is also seen that the dynamic stability zone of the flat composite panel is much smaller than those of the SMAHC panels. Therefore, the SMAHC panels always have superior dynamic stability compared with the composite panels, because they can survive much higher temperatures without the occurrence of flutter. The flutter boundaries of the composite flat panel were compared with those of Gou and Mei [25]. It was found that the present results are in good agreement with those of [25] until $\Delta T = 22.5°\text{C}$ (i.e., the critical buckling temperature of the composite-plate panel). At temperatures higher than $\Delta T = 22.5°\text{C}$, the present formulation is found to predict lower critical flutter values, because the effect of the static aerodynamic load after thermal buckling was neglected in the formulation presented in [25].

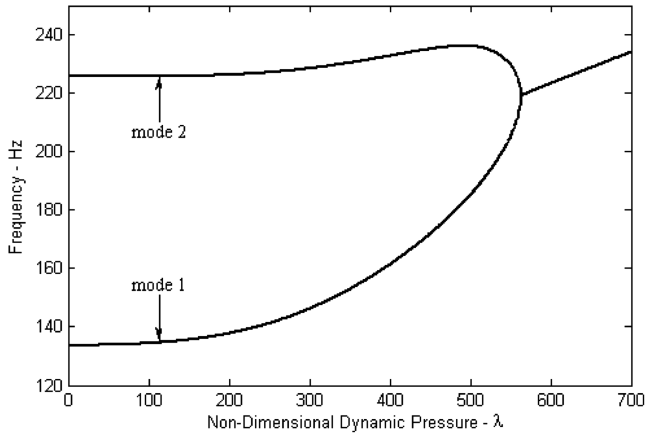

Fig. 9 Flutter coalescence curve for a clamped composite cylindrical panel with $H/h = 1$ and $\Delta T = 0°\text{C}$.

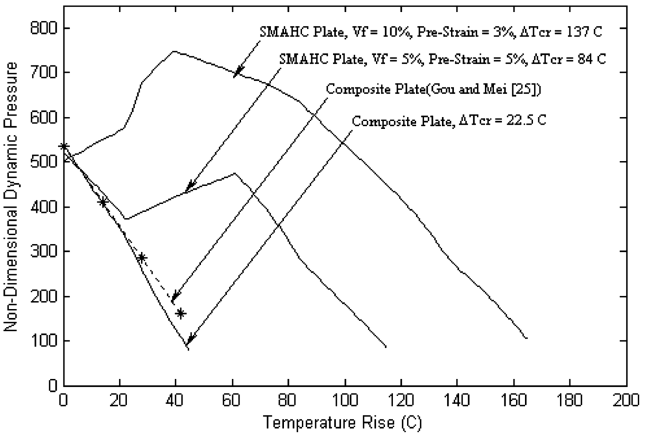

Fig. 10 Flutter boundaries of clamped composite and SMAHC plate panels.

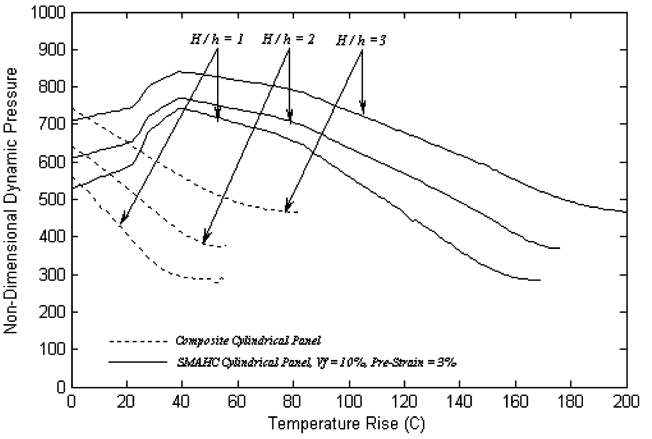

Fig. 11 Flutter boundaries of clamped composite and SMAHC cylindrical panels with different height-to-thickness ratios H/h.

Figure 11 illustrates the effect of height rise H/h and SMA fiber embeddings on the dynamic stability zone of curved panels. It is generally found that increasing the height rise value results in a more dynamically stable panel. In addition, the SMAHC cylindrical panels were found to survive much higher dynamic pressures and temperatures without suffering flutter instability.

V. Conclusions

A new nonlinear finite element formulation is presented to predict the thermal buckling and flutter boundaries of shape memory alloy hybrid composite cylindrical panels at elevated temperatures. The governing equations are obtained using Marguerre curved-plate theory and the principle of virtual work. The effect of large deflection is included in the formulation through the von Kármán nonlinear strain-displacement relations. The temperature dependence of material properties of the composite matrix and SMA fibers is considered in the formulation. The Newton–Raphson iteration method is employed to obtain the nonlinear deflections, and an eigenvalue problem is solved at each temperature rise to predict the flutter critical dynamic pressure. Results showed that increasing H/h value has a pronounced effect on the panel response through decreasing the postbuckling deflection especially at high temperatures as a result of the stiffness added due to panel curvature. At temperatures lower than the critical buckling values, the cylindrical SMAHC panels did not show a good performance compared with flat panels regarding thermal deflection. It is generally found that increasing the height rise value results in a more dynamically stable panel. Finally, it is concluded that the SMA fiber embeddings can be very useful in controlling the panel static thermal response through increasing the

buckling temperature and decreasing or suppressing the thermal postbuckling deflections. Moreover, the SMAHC panels are efficient in controlling flutter by highly increasing the flutter boundaries at elevated temperatures compared with those of the composite panels.

Acknowledgment

This work was supported by the BK21 program, Hanyang University, Seoul, Republic of Korea. The authors wish to express their gratitude for this financial support.

References

[1] Tauchart, T. R., "Thermally Induced Flexure, Buckling, and Vibration of Plates," *Applied Mechanics Reviews*, Vol. 44, No. 8, 1991, pp. 347–360.

[2] Thornton, E. A., "Thermal Buckling of Plates and Shells," *Applied Mechanics Reviews*, Vol. 46, No. 10, 1993, pp. 485–506.

[3] Gray, C. C., and Mei, C., "Finite Element Analysis of Thermal Postbuckling and Vibrations of Thermally Buckled Composite Plates," *Proceedings of the 32nd AIAA/ASME/ASCE/ AHS/ASC Structures, Structural Dynamics, and Materials Conference*, Pt. 4, AIAA, Washington, DC, 1991, pp. 2996–3007.

[4] Shi, Y., Lee, R. Y., and Mei, C., "Coexiting Thermal Post-Buckling of Composite Plates with Initial Imperfections Using Finite Element Modal Method," *Journal of Thermal Stresses*, Vol. 22, No. 6, 1999, pp. 595–614.

[5] Eslami, M. R., and Javaheri, R., "Buckling of Composite Cylindrical Shells Under Mechanical and Thermal Loads," *Journal of Thermal Stresses*, Vol. 22, 1999, pp. 527–545.

[6] Shen, H.-S., "Postbuckling Analysis of Pressure-Loaded Functionally Graded Cylindrical Shells in Thermal Environments," *Engineering Structures*, Vol. 25, 2003, pp. 487–497.

[7] Kadoli, R., and Ganesan, N., "Buckling and Free Vibration Analysis of Functionally Graded Cylindrical Shells Subjected to a Temperature-Specified Boundary Condition," *Journal of Sound and Vibration*, Vol. 289, 2006, pp. 450–480.

[8] Mei, C., Abdel-Motagaly, K., and Chen, R., "Review of Nonlinear Panel Flutter at Supersonic and Hypersonic Speeds," *Applied Mechanics Reviews*, Vol. 52, No. 10, 1999, pp. 321–332.

[9] Ibrahim, H. H., Tawfik, M., and Al-Ajmi, M., "Aero-Thermo-Mechanical Characteristics of Functionally Graded Material Panels with Temperature-Dependent Material Properties," *Proceedings of the 8th International Congress of Fluid Dynamics and Propulsion (ICFDP 8)*, American Society of Mechanical Engineers, ICFDP-EG-116, 2006.

[10] Ibrahim, H. H., Tawfik, M., and Al-Ajmi, M., "Non-Linear Panel Flutter for Temperature-Dependent Functionally Graded Material Panels," *Computational Mechanics*, Vol. 41, No. 2, 2008, pp. 325–334.

[11] Ibrahim, H. H., Tawfik, M., and Al-Ajmi, M., "Thermal Buckling and Nonlinear Flutter Behavior of Functionally Graded Material Panels," *Journal of Aircraft*, Vol. 44, No. 5, 2007, pp. 1610–1618.

[12] Singha, M. K., and Mandal, M., "Supersonic Flutter Characteristics of Composite Cylindrical Panel," *Composite Structures*, Vol. 82, 2008, pp. 295–301.

[13] Haddadpour, H., Mahmoudkhani, S., and Navazi, H. M., "Supersonic Flutter Prediction of Functionally Graded Cylindrical Shells," *Composite Structures*, Vol. 83, 2008, pp. 391–398.

[14] Birman, V., "Review of Mechanics of Shape Memory Alloy Structures," *Applied Mechanics Reviews*, Vol. 50, 1997, pp. 629–645.

[15] Lee, H. S., Lee, J. J., and Huh, J. S., "A Simulation Study on the Thermal Buckling Behavior of Laminated Composite Shells with Embedded Shape Memory Alloy (SMA) Wires," *Composite Structures*, Vol. 47, 1999, pp. 463–469.

[16] Tawfik, M., Ro, J. J., and Mei, C., "Thermal Post-Buckling and Aeroelastic Behavior of Shape Memory Alloy Reinforced Plates," *Smart Materials and Structures*, Vol. 11, 2002, pp. 297–307.

[17] Park, J. S., Kim, J. H., and Moon, S. H., "Vibration of Thermally Post-Buckled Composite Plates Embedded with Shape Memory Alloy Fibers," *Composite Structures*, Vol. 63, 2004, pp. 179–188.

[18] Roh, J. H., Oh, I. K., Yang, S. M., Han, J. H., and Lee, I., "Thermal Post-Buckling Analysis of Shape Memory Alloy Hybrid Composite Shell Panels," *Smart Materials and Structures*, Vol. 13, 2004, pp. 1337–1344.

[19] Ibrahim, H. H., Tawfik, M., and Negm, H. M., "Thermal Postbuckling and Flutter Behavior of Shape Memory Alloy Hybrid Composite Plates," *Proceedings of the 8th International Congress of Fluid Dynamics and Propulsion (ICFDP 8)*, American Society of Mechanical Engineers, Paper ICFDP-EG-153, 2006.

[20] Ibrahim, H. H., Tawfik, M., and Negm, H. M., "Thermo-Acoustic Random Response of Shape Memory Alloy Hybrid Composite Plates," *Journal of Aircraft*, Vol. 45, No. 3, 2008, pp. 962–970.

[21] Ibrahim, H. H., Tawfik, M., Yoo, H. H., and Lee, K. S., "Aero-Thermo-Mechanical Characteristics of Shape Memory Alloy Hybrid Composite Panels with Initial Geometric Imperfection," *Proceedings of the 15th International Congress on Sound and Vibration (ICSV15)* [CD-ROM], Daejeon, Republic of Korea, 2008.

[22] Azzouz, M. S., "Nonlinear Flutter of Curved Panels Under Yawed Supersonic Flow Using Finite Elements," Ph.D. Dissertation, Old Dominion Univ., Mechanical Engineering Dept., Norfolk, VA, 2005.

[23] Cross, W. B., Kariotis, A. H., and Stimeler, F. J., "Nitinol Characterization Study," NASA CR-14B, 1969.

[24] Gou, X., Przekop, A., and Mei, C., "Nonlinear Random Response of Shallow Shells at Elevated Temperatures Using Finite Element Modal Method," 45th AIAA/ASME/ASCE/ AHS/ASC Structures, Structural Dynamics, and Materials Conference, AIAA, Palm Springs, CA, 19–22 Apr. 2004, pp. 1558–1571.

[25] Gou, X., and Mei, C., "Application of Aeroelastic Modes on Nonlinear Supersonic Panel Flutter at Elevated Temperatures," *Computers and Structures*, Vol. 84, 2006, pp. 1619–1628.